Soft Matter

PAPER

View Article Online
View Journal

Cite this: DOI: 10.1039/d0sm00719f

Light-powered active colloids from monodisperse and highly tunable microspheres with a thin TiO_2 shell†

Pengzhao Xu, Shifang Duan, Zuyao Xiao, Zhou Yang and Wei Wang *

Received 21st April 2020,
Accepted 5th June 2020

DOI: 10.1039/d0sm00719f

rsc.li/soft-matter-journal

The emerging field of active matter, and its subset active colloid, is in great need of good model systems consisting of moving entities that are uniform and highly tunable. In this article, we address this challenge by introducing core–shell SiO_2–TiO_2 microspheres, prepared by chemically coating a thin layer of TiO_2 on an inert core, that are highly monodisperse in size (polydispersity 4.1%) and regular in shape (circularity 0.93). Compared with similar samples prepared by the classic sol–gel method, Janus TiO_2–Pt active colloids prepared with core–shell TiO_2 spheres move faster and boast a much clearer Janus interface. Moreover, a unique feature of these core–shell TiO_2 microspheres is their great tunability in the colloid size, shell thickness, and even the type of the core particle. These advantages are highlighted in two examples, one demonstrating a TiO_2–Pt active colloid with a magnetic core that enables magnetic manipulation, and the other demonstrating the collective expansion and contraction of a uniform cluster of core–shell TiO_2 colloids under UV light illumination. We believe that TiO_2 microspheres produced by this core–shell technique compare favorably with many other types of active colloids being employed as model systems, and thus open up many research possibilities.

1 Introduction

There has been mounting interest over the last decade in the interdisciplinary study of active matter,[1–8] entities that convert energy from their environment into mechanical motion while exhibiting interesting collective behaviors. Sitting at the core of active matter research is the development of model systems that, at a single-particle level, move autonomously, whereas inter-particle interactions at an ensemble level give rise to spatio-temporal patterns. Many popular model systems of active matter come from nature. Prominent examples include microorganisms, such as bacteria[9–11] and algae,[12] and biomolecules, such as motor proteins,[8] that spontaneously move, communicate, and organize.

The recent progress in the synthesis and manipulation of nanomaterials has enabled alternative model systems of active matter, in the form of colloidal particles that self-propel in water. These "active colloids"[13–18] are roughly micrometers in size and often move in water in a self-generated gradient[19] or by an externally applied force.[20] Compared with naturally occurring microswimmers and proteins, active colloids can be synthesized in large quantities, and tailored to specific needs *via* material functionalization. They are also easy to handle and visualize, and arguably require less expertise to master. Advantages like these have fueled the recent success of using active colloids as model systems to understand and manipulate active matter (see ref. 21 and references therein).

Active colloids powered by photochemical reactions combine the advantages of the phoretic interactions that give rise to rich, biomimetic collective behaviors, with the advantage of a remotely applied and tunable power source, and have thus emerged as an useful model system for active matter.[22] Notably, photocatalytic hematite (Fe_2O_3) Janus microparticles have been shown to spontaneously organize into living crystals[23,24] and gear superstructures,[25] while SiO_2 microspheres half coated with photocatalytic TiO_2 can assemble nearby passive tracer particles into crystalline structures.[26] Silver containing colloids show interesting, oscillatory behaviours and the emergence of waves under light illumination.[27–30] Despite this recent progress, the pursuit continues for a photochemically active colloid system that is clean, monodisperse, highly active, easy to synthesize, and tunable, highly desirable features that will certainly provide tremendous benefits to the study of active matter.

With this goal in mind, we focus on active colloids made of TiO_2, because it is a well-studied material with great tunability.

School of Materials Science and Engineering, Harbin Institute of Technology (Shenzhen), Shenzhen, 518055, China. E-mail: weiwangsz@hit.edu.cn

† Electronic supplementary information (ESI) available: Synthesis and experiment details, SEM micrographs, optical images and videos. See DOI: 10.1039/d0sm00719f

Even though a number of studies of TiO_2 active colloids have been published (see ref. 22 and 31 and references therein), particularly in the field of materials chemistry, TiO_2 microspheres used in these studies are typically smaller or close to 1 μm in diameter, not perfectly spherical, and polydisperse in size, limiting their usefulness for soft matter research. In this article, we report a different, core–shell approach (adapted from ref. 32) that produces highly active TiO_2 microspheres of much improved monodispersity and arbitrary particle size, by coating pre-synthesized or commercially available inert microspheres (core) with a thin, uniform layer of TiO_2 (shell). These advantages are highlighted by a comparison with TiO_2 microspheres fabricated by a sol–gel approach commonly found in the literature.[33,34] As active colloids, core–shell TiO_2 microspheres, and TiO_2–Pt Janus microspheres made from them, show uniform and consistent activity, at both individual and ensemble levels. Furthermore, to demonstrate the versatility of this core–shell synthesis, we showcase the ability to tune the particle sizes (and thus speed) and coat the spherical cores that are magnetic.

A particular emphasis is given throughout the article to improve the reproducibility of both particle synthesis and active colloid experiments, especially among soft matter chemists and physicists, and the related challenges are fully documented in the ESI.† Note that TiO_2–Pt microspheres that move autonomously under light will be referred in this article to as "motors" for the sake of simplicity.

2 Experimental

2.1 Materials

Ethanol (E111994 99.5%), formic acid (F112038 99%), hydroquinone (H_2Q H108945), tetrabutyl titanate (TBT T104105 99%) and titanium isopropoxide (TTIP T105735 95%) were purchased from Aladdin, China. Lutensol To-7 (9043-30-5, 99%) was purchased from Shandong Usolf Chemical Technology Co., Ltd of China. Silicon dioxide (SiO_2) microspheres (5 wt%) of various diameters were purchased from Huge Inc. China. Dynabeads (3742, 4–5 μm) were purchased from the BaseLine Chromtech Research Centre, China. All reagents were used without further purification.

2.2 Synthesis of core–shell TiO_2 microspheres (CS-TiO_2)

The following procedure is adapted from the literature,[32,35] and schematically illustrated in Fig. 1a. A more detailed schematic diagram is shown in Fig. S1 (ESI†). The expanded version with full details and precautions for the preparation process are also given in the ESI,† and are highly recommended to readers interested in reproducing our results.

Briefly, solution B (60 μL TBT and 2.5 mL ethanol) was added to violently shaken solution A (50 μL of SiO_2 microspheres, 30 μL of 0.1 M Lutensol To-7 and 2.5 mL of ethanol). TiO_2 nanoparticles were formed through alcoholysis condensation of the titanium source, and stabilized by the surfactant. Then, the mixture was sonicated for about 1 hour in a sonication bath to prevent aggregation, and allowed to sit for 1 h at room temperature for the reaction to complete. In this synthesis, the SiO_2 microsphere acted as a core on which TiO_2 nanoparticles were coated uniformly to form a TiO_2 shell. Finally, the SiO_2–TiO_2 core shell microspheres, short for CS-TiO_2, were obtained by centrifugation (shown in Fig. 1c), and re-suspended in 2.5 mL ethanol or de-ionized water for storage. Core–shell particles with different thicknesses of the TiO_2 shell can be synthesized by repeating the coating steps multiple times. Occasional cracking occurred for a CS-TiO_2 microsphere after repeated coating, presenting a rare opportunity to see the layered structure of a core–shell microsphere. An example is shown in Fig. 1d.

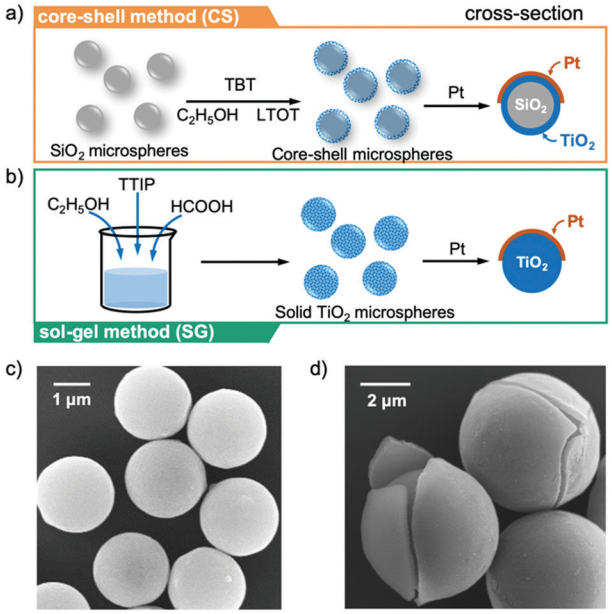

Fig. 1 Schematic of the synthesis of TiO_2–Pt Janus colloids by the core–shell (CS) method (a) or the sol–gel (SG) method (b). A thin Pt layer was coated by evaporation in both methods to produce TiO_2–Pt Janus microspheres. (c) SEM image of core–shell TiO_2 microspheres. (d) SEM image of a few cracked core–shell SiO_2–TiO_2 microspheres, obtained by coating 5 μm SiO_2 core 5 times.

2.3 Synthesis of TiO_2 microspheres by the sol–gel process (SG-TiO_2)

For the sol–gel method, the titanium source is hydrolyzed to generate a titanium precursor (sol), which then undergoes the sol–gel transition through condensation. The TiO_2 gel then grows gradually and is later calcined to form TiO_2 microspheres. In this study, we chose a non-aqueous sol–gel process following previous reports, considering the ease of synthesis and the sizes of the produced particles.[35,36] The brief synthesis procedure is as follows (illustrated in Fig. 1b): the mixture of 15 mL of ethanol (99.5%), 0.35 mL of formic acid and 0.65 mL of titanium isopropoxide (TTIP) was sealed in a Teflon-lined autoclave and heated at 150 °C for 1 h. Then, TiO_2 microspheres were cleaned with ethanol and de-ionized water and collected by centrifugation.

2.4 Preparation of TiO_2–Pt motors

To convert TiO_2 to the anatase phase, which has better photocatalytic properties, TiO_2 microspheres prepared by either method were slowly heated to 450 °C in a furnace at a ramp speed of 225 °C h^{-1}, annealed for 2 h, and then cooled to room temperature at the same ramp rate. TiO_2–Pt Janus microspheres were prepared by evaporating a 20 nm thick Pt layer on top of a monolayer of TiO_2 microspheres packed on a piece of Si wafer or a glass slide. A 5 nm thick layer of Cr was evaporated before Pt for better adherence. The SEM image of core–shell TiO_2–Pt microspheres is shown in Fig. S2 (ESI†). The Janus microspheres were then removed from the substrate by either mild sonication or gentle scraping, cleaned in water, and resuspended in de-ionized water for later use.

2.5 Characterization

X-ray diffraction (XRD) was performed on TiO_2 microspheres prepared by either method using a Rigaku D/Max 2500 PC X-ray diffractometer at a scanning rate of 7° min^{-1} from 10° to 80° (Cu-Kα irradiation, k = 1.54 Å). Scanning electron microscopy (SEM) was performed using a HitachiS-4700 scanning electron microscope. An inverted optical microscope (Olympus IX73) was used for observing and recording the particle motion. The UV-visible absorption spectrum of TiO_2 microspheres by either method was acquired on a UV-Vis spectrophotometer (Shimadzu UV-3600) (1.67 nm s^{-1}, 300–800 nm).

2.6 Activation and tracking of TiO_2–Pt motors

In a typical experiment, a drop of ~10 μL of TiO_2–Pt Janus microspheres was added to a pre-cleaned glass slide, and observed from the bottom with an inverted microscope. UV light of 365 nm (Thorlabs M365LP1) was applied from the top. Particle motion was recorded by using a CMOS camera (Point Gray, Grasshopper 3) typically at 30 frames per s. The recorded videos were then processed using homemade MATLAB codes (courtesy of Hepeng Zhang, Shanghai Jiaotong University), by which particle coordinates in the x–y plane were extracted. Particle instantaneous speeds at $t = i$ were calculated by the following equation $V_i = \sqrt{(x_{i+1} - x_i)^2 + (y_{i+1} - y_i)^2}/\Delta t$, where Δt = 1/30 s.

2.7 Data collection and analysis

Particle size measurement. Images acquired from SEM or OM were loaded in ImageJ,[37] from which after image processing the boundaries of any particle of a circularity above 0.8 were recognized. The particle diameter was determined by dividing the area of the recognized particle by π and taking square root. Particle size measurement was also performed using the dynamic light scattering technique, but the results were inconsistent across multiple measurements, and not used in this article. The size polydispersity was calculated by dividing the standard deviation by the average size.

Mean inter-particle distances in a cluster. The mass center of each particle in a cluster (*e.g.* Fig. 6) was connected by MATLAB *via* Delaunay triangulation. Then the average side length S_i of the ith particle was calculated. Finally, the mean distance $\bar{S}$ of each particle in a cluster of N particles was calculated by $\bar{S} = \sum S_i/N$. Particles along the outermost edge of the cluster as well as the particles with fewer than 6 neighbors were ignored.

3 Results

3.1 Material characterization and size uniformity

Size uniformity is a key feature of CS-TiO_2 microspheres, as highlighted in the size distribution measurements of both CS- and SG-TiO_2 microspheres (Fig. 2a and b). Scanning electron microscopy (SEM) and optical microscopy (OM) images were recorded for the same sample (Fig. 2a), and particle diameters and circularity were acquired using ImageJ. The diameters of the pure SiO_2 microspheres used as the core for CS-TiO_2 microspheres were also measured for reference. Colloid sizes measured from OM images, shown in the bottom panel in Fig. 2b, are clearly larger than their actual sizes, likely because of the poorly defined particle boundaries under an OM, which lead to errors in image recognition. Taking SEM images as a more accurate assessment (Fig. 2b, top panel), the

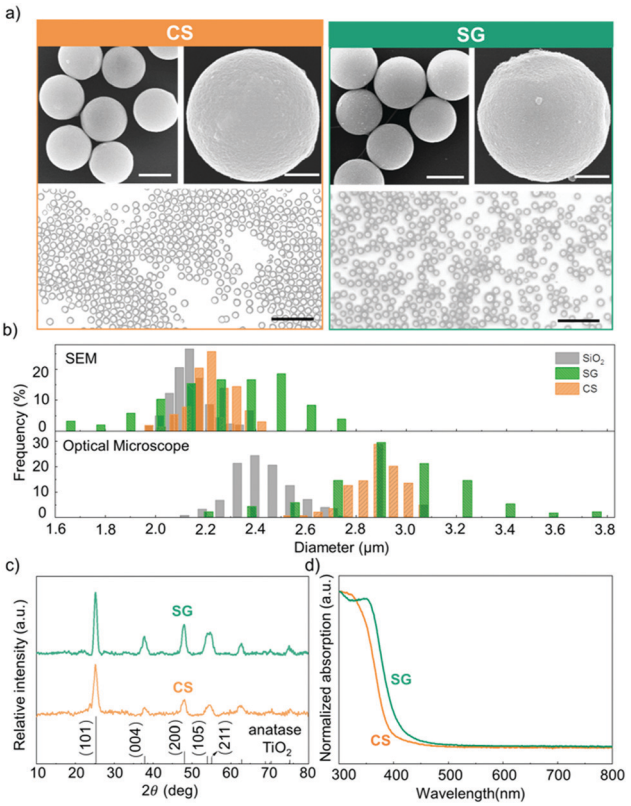

Fig. 2 Characterization of TiO_2 microspheres prepared by the core–shell (CS) and sol–gel (SG) method. (a) SEM (top) and OM (bottom) images of TiO_2 microspheres. Scale bars represent 2 μm, 0.5 μm and 10 μm in each of the three panels. (b) Particle size distribution of SiO_2 and TiO_2 microspheres (both CS- and SG-), measured by images from SEM (top) and OM (bottom). (c) XRD patterns correspond to the anatase phase. (d) UV-Vis adsorption spectra.

diameters of SiO_2, CS-TiO_2 and SG-TiO_2 microspheres were determined to be 2.14 ± 0.07 μm, 2.23 ± 0.09 μm and 2.33 ± 0.25 μm, respectively. Overall, the particle size measurements show that the size distribution of CS-TiO_2 microspheres, with a thin TiO_2 layer of ~90 nm thickness, is narrower than that of SG-TiO_2, with a size polydispersity of 4.1% *vs.* 10.9%. The circularity of CS- and SG-TiO_2 microspheres is 0.93 and 0.91, respectively.

Some additional material characterization was performed on both CS- and SG-TiO_2 microspheres, and the results are shown in Fig. 2c and d. Fig. 2c shows that TiO_2 microspheres synthesized by either method and after annealing at 450 °C are of anatase phase with good crystallinity. Being anatase phase TiO_2 is known to be critical for efficient photoactivity.[38] The results of ultraviolet-visible spectroscopy (UV-Vis) in Fig. 2d show that both CS- and SG-TiO_2 microspheres absorb light strongly in the UV regime (<400 nm), typical for this material with a bandgap of ~3.2 eV. Notably, the absorption of CS-TiO_2 microspheres shifts slightly to blue, possibly arising from the differences in the synthesis of these two samples and their defect properties.[39] Finally, zeta potential measurements show that both the CS- and SG-TiO_2 microspheres were negatively charged in aqueous solutions, with a zeta potential of −42.4 mV and −43.7 mV, respectively. Although a detailed investigation of these material properties is beyond the scope of this article, the important message, at least for readers interested in using CS-TiO_2 microspheres for active colloid research, is that they are made of practically the same material as their sol–gel counterparts.

3.2 Single particle propulsion

In this section, we report the photo-electrochemical propulsion of TiO_2–Pt motors, which were fabricated by coating CS- or SG-TiO_2 microspheres with a thin Pt layer (see the Experimental section for details). Our main findings, detailed below, are that, compared with their sol–gel counterparts, CS-TiO_2–Pt motors move with a significantly faster speed, a similar speed variation, and a much clearer Janus interface.

We begin by briefly reviewing the propulsion mechanism of a TiO_2–metal Janus microsphere (Fig. 3a), applicable to both CS- and SG-TiO_2 microspheres. This mechanism is well established in the literature.[31,40–42] Upon irradiation of light of proper wavelengths (typically in the UV regime, see UV-vis measurement in Fig. 2d), electrons in the valence band of TiO_2 are excited into the conduction band, leaving holes. With the presence of a noble metal layer on the TiO_2 surface, such as gold or platinum, a Schottky junction at the metal–TiO_2 interface is formed that attracts electrons to the metal, leading to the so-called electron–hole separation. Electrons then reduce chemicals at the metal–solution interface, while holes oxidize chemicals at the TiO_2–solution interface. In the case of pure water, the redox pairs essentially form water electrolysis:

$$\text{Anode } (TiO_2)\text{: } 2H_2O + 4h^+ \rightarrow 4H^+ + O_2 \quad (1)$$

$$\text{Cathode (Pt): } 4H^+ + 4e^- \rightarrow 2H_2 \quad (2)$$

This pair of reaction results in different H^+ concentrations near the two caps of the Janus sphere, thus forming an external

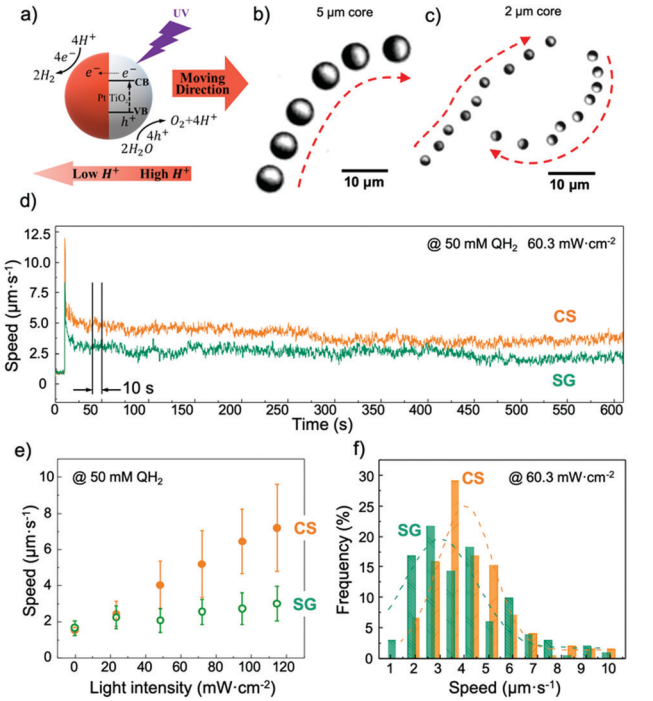

Fig. 3 Single particle dynamics of TiO_2–Pt motors. (a) Schematic diagram of the propulsion mechanism of TiO_2–Pt colloids in water. Stacked optical micrographs of the CS-TiO_2–Pt motors made of (b) 5 μm SiO_2 cores moving in water for 13.4 s and (c) 2 μm SiO_2 cores moving in water for 6 s. (d) Temporal evolution of the speeds of CS- or SG-TiO_2–Pt colloids for 10 min after illumination. Error bars represent the standard deviation of more than 50 colloids in either case. (e) Averaged speeds of CS- or SG-TiO_2–Pt colloids within 10 s marked in (d) at different light intensities. (f) Speed distribution of CS- or SG-TiO_2–Pt motors, illuminated at 60.3 mW cm^{-2}, within 10 s marked in (d). Experimental conditions are labeled in each plot.

electric field pointing to the Pt side from the TiO_2 side. Because a TiO_2–Pt microsphere is negatively charged, it moves towards the TiO_2 side in a way similar to electrophoresis. This mechanism is thus termed self-electrophoresis[22,31] and is also responsible for the propulsion of bimetallic colloids moving in H_2O_2.[43,44]

In practice, however, pure water is less commonly used as the fuel for such photochemical TiO_2–Pt motors, because propulsion is typically slow. Rather, H_2O_2 is a common alternative due to its favorable electrochemical potential at both the cathode and anode:

$$\text{Anode } (TiO_2)\text{: } H_2O_2 + 2h^+ \rightarrow 2H^+ + O_2 \quad (3)$$

$$\text{Cathode (Pt): } H_2O_2 + 2e^- \rightarrow 2OH^- \quad (4)$$

However, the use of H_2O_2 also leads to other practical issues. First, the decomposition of H_2O_2 produces O_2 that eventually forms bubbles and obstructs experiments. A low concentration of H_2O_2 and a low population density of motors could mitigate this issue to a certain extent. Second, we have found that TiO_2–Pt colloids, upon illumination, move out of focus followed by sudden movement towards the substrate and becoming stuck on it. This peculiar "lift-off" remains to be understood

(possibly connected to its bottom-heaviness[45–47]), but obviously causes a severe problem for many studies. To circumvent these issues, and inspired by recent studies from the Tang lab,[48–50] we have in our experiments used hydroquinone (QH_2) as an alternative fuel, which forms a redox pair with its oxidized form benzoquinone (BQ):

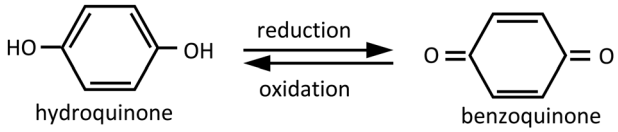

$$\text{Anode } (TiO_2)\text{: } QH_2 + 2h^+ \rightarrow BQ + 2H^+ \quad (5)$$

$$\text{Cathode (Pt): } BQ + 2H^+ + 2e^- \rightarrow QH_2 \quad (6)$$

Just like water or H_2O_2, a proton gradient is still responsible for the photochemical propulsion of TiO_2–Pt colloids in QH_2 by the same self-electrophoresis mechanism. In the remainder of this article, aqueous solution containing 50 mM QH_2 was used as the fuel, unless otherwise noted, and minimal bubble or unwanted lift-off was observed. This chemical can be easily purchased from major chemical vendors, and is highly recommended for readers interested in reproducing our results. Note that both H_2O_2 and hydroquinone are considered hazardous chemicals that cause serious eye damage and allergic skin reactions, among other health issues. Proper care is therefore needed when handling these chemicals (see safety data sheet available online for details).

Typical single-particle dynamics of a TiO_2–Pt active colloid in QH_2 solution is as follows. Because these particles are much heavier than water, they naturally settle down at the bottom of the observation chamber and are observed from below. Upon turning on the UV light, TiO_2–Pt Janus microspheres immediately sprang into action, and explored the *xy* 2D plane in random trajectories at a speed of a few μm s^{-1} with their TiO_2 caps moving forward (Video S1, ESI†). Their trajectories were largely uncorrelated with each other at dilute concentrations of particles, but clusters did appear at higher densities (results now shown here). A key advantage of CS-TiO_2–Pt Janus motors over their sol–gel counterparts is the clear visualization of the Janus interface that separates the TiO_2 and the metal cap. This is an important feature for many soft matter studies where the rotational diffusion, directionality or tilting of a Janus active colloid is concerned.[51–55] Because transmissive light was used in our experiments, transparent TiO_2 hemispheres appeared bright, while the metal cap appeared dark, a feature clearly seen in Fig. 3b and c. This kind of clear Janus interface is, however, not easily distinguishable for SG-TiO_2–Pt (see Fig. S3, ESI†), possibly related to how light interacts with a solid TiO_2 sphere.

A notable feature for TiO_2–Pt motors fabricated by either method is that they dash at the moment of turning on light, *i.e.* an instantaneous speed that increases sharply after applying light (discussed in more detail in the ESI†), then decreases rapidly over a few seconds before plateauing to a stable speed that is $<50\%$ of the initial peak. A representative temporal evolution of the speed profile, for both CS- and SG-TiO_2–Pt motors, is given in Fig. 3d. Such a slow but steady change in particle speeds obviously puts a limit to long time observations. For these studies, we recommend users to wait for the system to stabilize for at least 30 s before recording, so that the speeds of motors do not appreciably decrease during an experiment. Following this recommendation, we obtained and compared in Fig. 3e and f the speeds for CS- and SG-TiO_2–Pt colloids averaged within a 10 s window. The results, shown in Fig. 3e for various light intensities, are that TiO_2–Pt colloids made of the core–shell method consistently outperform their sol–gel counterparts, reaching a peak speed of 7.2 μm s^{-1} and 3.0 μm s^{-1}, respectively at a light intensity of 114.8 mW cm^{-2}. We do not understand why one moves faster than the other, but suspects that this is connected to surface morphology or how light is absorbed in a thin shell *vs.* a solid sphere. Surprisingly, despite the much better size uniformity of core–shell colloids, a population of them still moved with a wide distribution of speeds similar to their sol–gel counterparts. This poor distribution of both types of colloids, shown Fig. 3f for a particular light intensity, suggests that the seemingly uniform population of core–shell colloids could in fact be quite heterogeneous in coating thickness or qualities, an important issue for experimentalists to note.

3.3 Tunability

One great benefit conferred by photochemically active colloids, compared with those powered by other mechanisms, is their tunability. This is manifested in multiple ways. For example, the speeds of photochemically active colloids can be tuned, and their on/off can be switched, by modulating light remotely and continuously, as demonstrated by many existing studies.[30,33,42,56] Beyond the apparent light modulation, TiO_2–metal motors fabricated by the core–shell method offer the unique advantage of structural tunability, in the thickness of the TiO_2 layer, in the diameter of the inert SiO_2 core, and even in the material of the core. This portfolio of excellent adjustability, detailed below, offers unprecedented freedom for customizing an active colloid system for a specific study.

First, the thickness of the TiO_2 shell of a SiO_2–TiO_2 core–shell microsphere can be increased by repeatedly coating the same samples with multiple layers of TiO_2. For example, in Fig. 4a we show that after each coating, the thickness of the TiO_2 shell increases in a roughly linear fashion with the number of repetitions. By the end of the fifth coating, a TiO_2 shell of $\sim$400 nm thickness was obtained. This translates to a thickness of 90 nm for each layer of the TiO_2 shell, agreeing with the particle size measurement in Fig. 2b. Meanwhile, the speed of the active colloids also roughly scales linearly with the number of TiO_2 layers. This is perhaps not surprising; with the increase of the TiO_2 shell thickness, there is more active material generating electrons and holes, leading to a larger concentration gradient and faster propulsion. There is inevitably an increase in the hydrodynamic drag as the shell gets

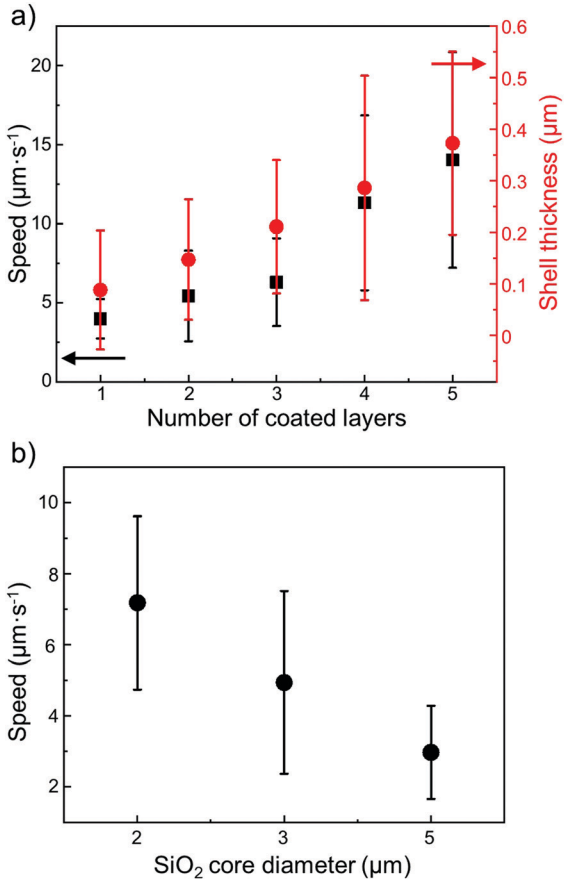

Fig. 4 Tuning the speeds of core–shell TiO_2–Pt colloids. (a) Average speeds after coating 2 μm SiO_2 with TiO_2 layers multiple times. (b) Average speeds after coating 1 layer of TiO_2 on SiO_2 cores of different sizes. Experiments in (a and b) were performed in 50 mM of QH_2 and at 60.3 mW cm^{-2} of light intensity.

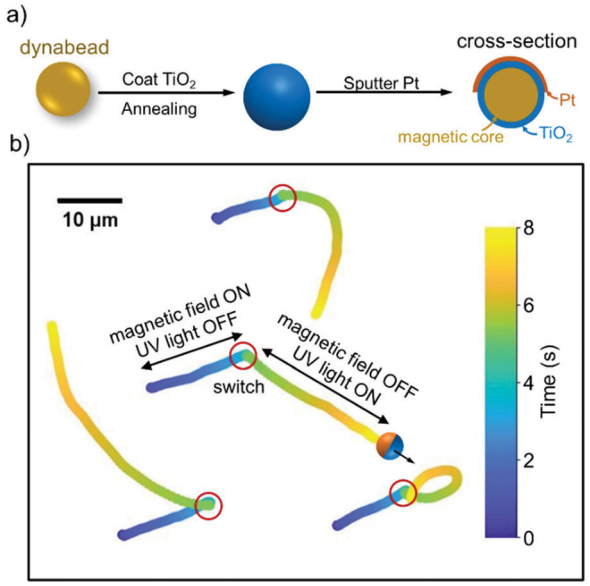

Fig. 5 Core–shell TiO_2 microspheres with a magnetic core. (a) Schematic for coating a dynabead (magnetic microsphere) with a thin TiO_2 shell to obtain a dynabead-TiO_2–Pt Janus microsphere. (b) Tracked trajectories of dynabead-TiO_2–Pt colloids during 7.7 s.

thicker, but that seems to be a minor effect compared with the increase in the propulsive force.

The second way to tune the structure, and hence the activity of a TiO_2 microsphere, is to change the size of the inert SiO_2 cores. Fig. 4b shows that TiO_2–Pt motors made of larger SiO_2 cores moved more slowly: a TiO_2–Pt colloid with a 5 μm SiO_2 core moved with an average speed of ~3 μm s^{-1}, while a smaller TiO_2–Pt with a 2 μm SiO_2 core moved at 7 μm s^{-1}. This trend that the colloid speed scales inversely to its size is in agreement with earlier studies of chemically powered active colloids.[57,58]

The third, and perhaps the most interesting, way to tune the behaviors of a TiO_2 microsphere is to replace the SiO_2 core with a particle of different materials or shapes. After coating, a core–shell TiO_2 microsphere would in principle retain the shape, monodispersity, and physical properties of the original core. As an example, we have chosen a dynabead (a SiO_2 microsphere decorated with iron oxide) as the core, since it is one of the most commonly used microspheres, and easy to identify whether the magnetic core has been successfully encapsulated. By going through the same coating procedure described above, the obtained dynabead-TiO_2 core–shell microspheres were both magnetic and photoactive (see Fig. S4 (ESI†) for microscopic images). By further sputtering Pt, a dynabead-TiO_2–Pt Janus microsphere moved under UV illumination, while being subjected to magnetic manipulation. Representative trajectories of a few such microspheres under a magnetic field (from a handheld magnet) and under UV illumination are shown in Fig. 5, which are clearly divided into a first, dark segment of linear, concerted motion (magnetic field on and UV off), and a second, illuminated segment that is randomized and curvy (magnetic field off and UV on). The encapsulation of a magnetic core provides an additional dimension of control over the speed, directionality, orientation, or inter-particle interactions of photoactive colloids. Furthermore, microparticles of other shapes, sizes, materials or even surface chemistry can be in principle encapsulated by the same process (with a possible modification of the protocol), but is not explored in the current study. Note that because calcination at 450 °C is needed in particle synthesis, the core needs to be heat resistant at this temperature, thus excluding those made of polymer.

3.4 Collective behaviors

The study of collective behaviors of active colloids has received considerable interest among soft matter physicists because of its relevance to the general topic of active matter.[17,59] It is also useful in the context of swarm robotics and biomimetic materials,[60–63] and is thus a popular topic among a wide range of disciplines. To highlight the usefulness of core–shell TiO_2 microspheres in the study of collective behaviors, in this section we show how a dense population of them (not Janus particles) aggregate and disperse on cue (see Video S2, ESI†), with an emphasis on cluster uniformity.

In the following experiment, CS-SiO_2–TiO_2 microspheres with a thick TiO_2 shell were fabricated by repeatedly coating a

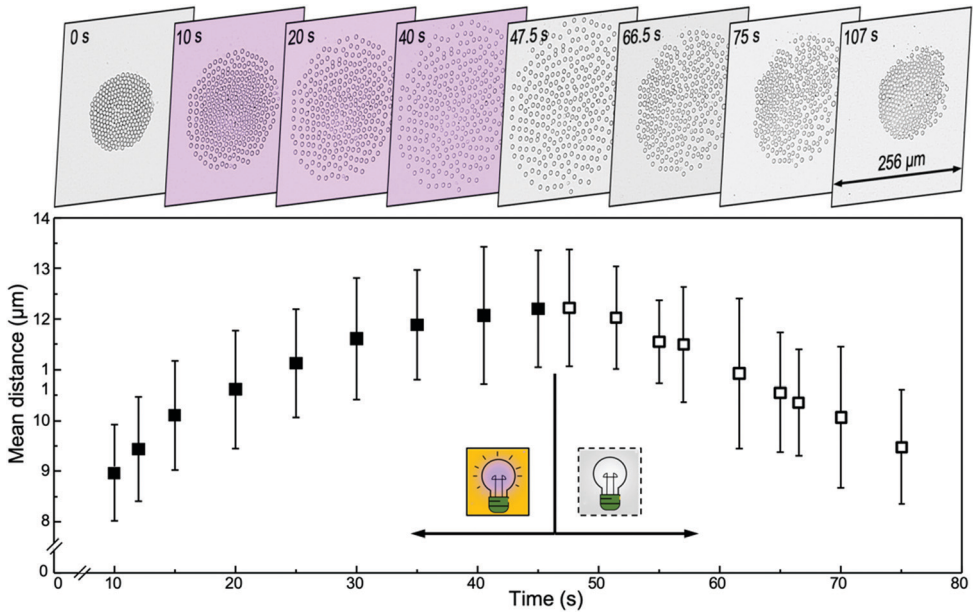

Fig. 6 Expansion and contraction of a cluster of core–shell SiO_2–TiO_2 microspheres (not Janus). Time-elapsed optical micrographs of this cluster surround a data plot of the temporal evolution of the mean distance of the constituent particles ($\bar{S}$, see the Experimental section for details). Solid and hollow data points correspond to light on and off, respectively.

5 μm SiO_2 core with a total of 5 layers of TiO_2. They were dispersed in 5% H_2O_2 solutions. Under weak ambient lighting provided by a white LED, they spontaneously and slowly aggregated into tight, round clusters with local crystalline domains, shown in Fig. 6 (t = 0). Upon turning on UV light (365 nm and 114.8 mW cm^{-2}), these clusters of CS-TiO_2 microspheres immediately expanded, until a loose yet stable cluster of semi-regular inter-particle spacing was formed after ~40 s. This expanded cluster, upon switching the light off (leaving the ambient lighting on), contracted again into a tight, semi-crystalline cluster in ~60 s. Ref. 64 and 65 give a qualitative mechanism that attributes the spontaneous clustering of TiO_2 microspheres in the dark to the dissociation and diffusion of protons from the TiO_2 surface, and the resulting electroosmosis. The illuminated expansion, on the other hand, is argued to arise from the photochemical decomposition of H_2O_2 and the resulting O_2 concentration gradient.

Although the same observation has been reported by the Sen group with both AgCl[28,66] and TiO_2 microparticles,[64] and again more recently by Mou *et al.*[65] with TiO_2 microspheres, what stands out in our demonstration is an un-paralleled uniformity in the shape and size of TiO_2 microspheres that gave rise to close-packed clusters when contracted, and regular inter-particle spacing when expanded. This feature significantly facilitates fast and accurate quantitative analysis used in many soft matter physics studies. The changes in the mean inter-particle distances of this cluster during this cycle are shown in Fig. 6 as a rather rudimentary example of such a quantitative analysis.

4. Conclusions

To summarize, we have reported core–shell (CS) SiO_2–TiO_2 microspheres prepared by chemically coating a thin layer of TiO_2 on an inert core, adapted from a previously reported protocol. A CS-TiO_2–Pt Janus microsphere, fabricated by further coating half of the core–shell sphere with Pt, moves in water, dilute H_2O_2 or dilute hydroquinone (QH_2) solutions *via* self-electrophoresis under light illumination. By comparing with similar TiO_2 microspheres synthesized by the classic sol–gel method, the main advantages, and thus the usefulness in soft matter research, of the core–shell SiO_2–TiO_2 microspheres reported here are (1) a high monodispersity in particle size (polydispersity 4.1%); (2) particles of nearly spherical shapes and smooth surfaces; (3) good photochemical performance and a clear Janus interface as active colloids, and (4) great tunability in colloid sizes, speeds and functionalities, by varying the number of TiO_2 layers, the size of the core microspheres, or even the type of particles being encapsulated. These attractive features become clear after a series of material characterization and motion analysis, culminating in one example of a core–shell TiO_2 colloid with a magnetic core, and a second demonstration of the collective expansion and contraction of a uniform cluster of core–shell TiO_2 microspheres.

There are certainly limitations to these core–shell TiO_2 particles. For example, they are more difficult and time-consuming to synthesize and purify compared to many other types of active colloids, and a good amount of trials and errors are needed to overcome the learning curve. Moreover, they are still haunted by the same practical issues associated with photochemically powered active colloids, such as a dash that moves the particle out of focus when light is turned on, an inability to move at high ionic strength (not shown here), and the requirement of a UV light source. These limitations, fully documented in the ESI,† and currently being addressed by us and many others working in the field, are a testimony that no system is perfect.

Despite these limitations, we advocate that the reported core–shell TiO_2 microsphere, powered and modulated by light, is of high practical value as a good model system for active colloids and active matter. For example, the clear Janus interface and fast propulsion make studies of individual dynamics easy, while high particle uniformity greatly facilitates the statistical analysis of ensemble dynamics and collective behaviors. Importantly, the much greater tunability endowed by this core–shell method than most other methods for synthesizing active colloids, especially the capability of substituting the core, offers a tremendous amount of research possibilities. For example, by coating a colloidal particle of a unique shape or electromagnetic properties, synthesized separately, with TiO_2 and thus endowing it with photoactivity, interesting collective behaviors can be explored in a complex energy landscape.

Conflicts of interest

There are no conflicts to declare.

Acknowledgements

This project is financially supported by the Science Technology and Innovation Program of Shenzhen (JCYJ20190806144807401), the Natural Science Foundation of Guangdong Province (No. 2017B030306005), and the National Natural Science Foundation of China (11774075). We thank Prof. Penger Tong and Hepeng Zhang for inspiring discussions and sample-testing, and our (past and present) lab members for proof-reading and wonderful suggestions.

Notes and references

1 D. Needleman and Z. Dogic, *Nat. Rev. Mater.*, 2017, **2**, 1–14.
2 J. M. Yeomans, *Nat. Mater.*, 2014, **13**, 1004–1005.
3 M. C. Marchetti, J.-F. Joanny, S. Ramaswamy, T. B. Liverpool, J. Prost, M. Rao and R. A. Simha, *Rev. Mod. Phys.*, 2013, **85**, 1143.
4 G. De Magistris and D. Marenduzzo, *Phys. A*, 2015, **418**, 65–77.
5 N. T. Ouellette, *Matter*, 2019, **1**, 297–299.
6 J. M. Yeomans, *Europhys. News*, 2017, **48**, 21–25.
7 G. Popkin, *Nat. News*, 2016, **529**, 16.
8 T. Sanchez, D. T. Chen, S. J. DeCamp, M. Heymann and Z. Dogic, *Nature*, 2012, **491**, 431–434.
9 M. F. Copeland and D. B. Weibel, *Soft Matter*, 2009, **5**, 1174–1187.
10 H.-P. Zhang, A. Be'er, E.-L. Florin and H. L. Swinney, *Proc. Natl. Acad. Sci. U. S. A.*, 2010, **107**, 13626–13630.
11 T. Turiv, R. Koizumi, K. Thijssen, M. M. Genkin, H. Yu, C. Peng, Q.-H. Wei, J. M. Yeomans, I. S. Aranson and A. Doostmohammadi, 2020, arXiv preprint arXiv:2001.05622.
12 A. P. Petroff, X.-L. Wu and A. Libchaber, *Phys. Rev. Lett.*, 2015, **114**, 158102.
13 I. S. Aranson, *Phys.-Usp.*, 2013, **56**, 79.
14 J. Zhang, E. Luijten, B. A. Grzybowski and S. Granick, *Chem. Soc. Rev.*, 2017, **46**, 5551–5569.
15 S. Ebbens, *Curr. Opin. Colloid Interface Sci.*, 2016, **21**, 14–23.
16 C. Bechinger, R. Di Leonardo, H. Löwen, C. Reichhardt, G. Volpe and G. Volpe, *Rev. Mod. Phys.*, 2016, **88**, 045006.
17 A. Zöttl and H. Stark, *J. Phys.: Condens. Matter*, 2016, **28**, 253001.
18 B. Liebchen and H. Löwen, *Acc. Chem. Res.*, 2018, **51**, 2982–2990.
19 W. Wang, W. Duan, S. Ahmed, T. E. Mallouk and A. Sen, *Nano Today*, 2013, **8**, 531–554.
20 T. Xu, W. Gao, L. P. Xu, X. Zhang and S. Wang, *Adv. Mater.*, 2017, **29**, 1603250.
21 W. Wang, X. Lv, J. L. Moran, S. Duan and C. Zhou, *Soft Matter*, 2020, **16**, 3846–3868.
22 J. Wang, Z. Xiong, J. Zheng, X. Zhan and J. Tang, *Acc. Chem. Res.*, 2018, **51**, 1957–1965.
23 J. Palacci, S. Sacanna, A. P. Steinberg, D. J. Pine and P. M. Chaikin, *Science*, 2013, **339**, 936–940.
24 J. Palacci, S. Sacanna, S.-H. Kim, G.-R. Yi, D. Pine and P. Chaikin, *Philos. Trans. R. Soc., A*, 2014, **372**, 20130372.
25 A. Aubret, M. Youssef, S. Sacanna and J. Palacci, *Nat. Phys.*, 2018, **14**, 1114–1118.
26 D. P. Singh, U. Choudhury, P. Fischer and A. G. Mark, *Adv. Mater.*, 2017, **29**, 1701328.
27 C. Zhou, N. J. Suematsu, Y. Peng, Q. Wang, X. Chen, Y. Gao and W. Wang, *ACS Nano*, 2020, **14**, 5360–5370.
28 M. E. Ibele, P. E. Lammert, V. H. Crespi and A. Sen, *ACS Nano*, 2010, **4**, 4845–4851.
29 C. Zhou, X. Chen, Z. Han and W. Wang, *ACS Nano*, 2019, **13**, 4064–4072.
30 X. Chen, C. Zhou, Y. Peng, Q. Wang and W. Wang, *ACS Appl. Mater. Interfaces*, 2020, **12**, 11843–11851.
31 L. Xu, F. Mou, H. Gong, M. Luo and J. Guan, *Chem. Soc. Rev.*, 2017, **46**, 6905–6926.
32 A. F. Demirörs, A. van Blaaderen and A. Imhof, *Langmuir*, 2010, **26**, 9297–9303.
33 B. Jang, A. Hong, H. E. Kang, C. Alcantara, S. Charreyron, F. Mushtaq, E. Pellicer, R. Büchel, J. Sort, S. S. Lee, B. J. Nelson and S. Pané, *ACS Nano*, 2017, **11**, 6146–6154.
34 Z. Deng, F. Mou, S. Tang, L. Xu, M. Luo and J. Guan, *Appl. Mater. Today*, 2018, **13**, 45–53.
35 S. Eiden-Assmann, J. Widoniak and G. Maret, *Chem. Mater.*, 2004, **16**, 6–11.
36 K. He, G. Zhao and G. Han, *CrystEngComm*, 2014, **16**, 7881–7884.
37 M. D. Abràmoff, P. J. Magalhães and S. J. Ram, *Biophotonics Int.*, 2004, **11**, 36–42.
38 A. Fujishima and K. Honda, *Nature*, 1972, **238**, 37–38.
39 S. Yu, B. Han, Y. Lou, G. Qian and Z. Wang, *Inorg. Chem.*, 2020, **59**, 3330–3339.
40 L. Kong, C. C. Mayorga-Martinez, J. Guan and M. Pumera, *ACS Appl. Mater. Interfaces*, 2018, **10**, 22427–22434.
41 F. Mou, L. Kong, C. Chen, Z. Chen, L. Xu and J. Guan, *Nanoscale*, 2016, **8**, 4976–4983.
42 T. Maric, M. Z. M. Nasir, R. D. Webster and M. Pumera, *Adv. Funct. Mater.*, 2020, **30**, 2000112.

43 W. F. Paxton, K. C. Kistler, C. C. Olmeda, A. Sen, S. K. St. Angelo, Y. Cao, T. E. Mallouk, P. E. Lammert and V. H. Crespi, *J. Am. Chem. Soc.*, 2004, **126**, 13424–13431.
44 S. Fournier-Bidoz, A. C. Arsenault, I. Manners and G. A. Ozin, *Chem. Commun.*, 2005, 441–443.
45 A. I. Campbell and S. J. Ebbens, *Langmuir*, 2013, **29**, 14066–14073.
46 A. Rashidi, S. Razavi and C. L. Wirth, *Phys. Rev. E*, 2020, **101**, 042606.
47 D. P. Singh, W. E. Uspal, M. N. Popescu, L. G. Wilson and P. Fischer, *Adv. Funct. Mater.*, 2018, **28**, 1706660.
48 J. Zheng, J. Wang, Z. Xiong, Z. Wan, X. Zhan, S. Yang, J. Chen, J. Dai and J. Tang, *Adv. Funct. Mater.*, 2019, **29**, 1901768, DOI: 10.1002/adfm.201901768.
49 B. Dai, J. Wang, Z. Xiong, X. Zhan, W. Dai, C. C. Li, S. P. Feng and J. Tang, *Nat. Nanotechnol.*, 2016, **11**, 1087–1092.
50 J. Wang, Z. Xiong, X. Zhan, B. Dai, J. Zheng, J. Liu and J. Tang, *Adv. Mater.*, 2017, **29**, 1701451.
51 F. Ginot, I. Theurkauff, F. Detcheverry, C. Ybert and C. Cottin-Bizonne, *Nat. Commun.*, 2018, **9**, 1–9.
52 M. Tătulea-Codrean and E. Lauga, *J. Fluid Mech.*, 2018, **856**, 921–957.
53 S. Das, A. Garg, A. I. Campbell, J. Howse, A. Sen, D. Velegol, R. Golestanian and S. J. Ebbens, *Nat. Commun.*, 2015, **6**, 8999.
54 M. N. Popescu, W. E. Uspal, A. Dominguez and S. Dietrich, *Acc. Chem. Res.*, 2018, **51**, 2991–2997.
55 J. Simmchen, J. Katuri, W. E. Uspal, M. N. Popescu, M. Tasinkevych and S. Sanchez, *Nat. Commun.*, 2016, **7**, 10598.
56 Q. Wang, C. Wang, R. Dong, Q. Pang and Y. Cai, *Inorg. Chem. Commun.*, 2018, **91**, 1–4.
57 P. M. Wheat, N. A. Marine, J. L. Moran and J. D. Posner, *Langmuir*, 2010, **26**, 13052–13055.
58 S. Ebbens, M.-H. Tu, J. R. Howse and R. Golestanian, *Phys. Rev. E: Stat., Nonlinear, Soft Matter Phys.*, 2012, **85**, 020401.
59 J. Elgeti, R. G. Winkler and G. Gompper, *Rep. Prog. Phys.*, 2015, **78**, 056601.
60 J. Yu, D. Jin, K.-F. Chan, Q. Wang, K. Yuan and L. Zhang, *Nat. Commun.*, 2019, **10**, 1–12.
61 Y. Yang and M. A. Bevan, *Sci. Adv.*, 2020, **6**, eaay7679.
62 D. Jin, J. Yu, K. Yuan and L. Zhang, *ACS Nano*, 2019, **13**, 5999–6007.
63 H. Xie, M. Sun, X. Fan, Z. Lin, W. Chen, L. Wang, L. Dong and Q. He, *Sci. Rob.*, 2019, **4**, eaav8006.
64 Y. Hong, M. Diaz, U. M. Córdova-Figueroa and A. Sen, *Adv. Funct. Mater.*, 2010, **20**, 1568–1576.
65 F. Mou, J. Zhang, Z. Wu, S. Du, Z. Zhang, L. Xu and J. Guan, *iScience*, 2019, **19**, 415–424.
66 M. Ibele, T. E. Mallouk and A. Sen, *Angew. Chem., Int. Ed.*, 2009, **48**, 3308–3312.